Nanoscale

Orthogonal Deposition of Au on Different Facets of Ag Cuboctahedra for the Fabrication of Nanoboxes with Complementary Surfaces

Journal:	*Nanoscale*
Manuscript ID	NR-ART-09-2019-008420.R2
Article Type:	Paper
Date Submitted by the Author:	19-Nov-2019
Complete List of Authors:	Ahn, Jaewan; Georgia Institute of Technology, Materials Science and Engineering Kim, Junki; Georgia Institute of Technology, Materials Science and Engineering Qin, Dong; Georgia Institute of Technology, Materials Science and Engineering

Orthogonal Deposition of Au on Different Facets of Ag Cuboctahedra for the Fabrication of Nanoboxes with Complementary Surfaces

*Jaewan Ahn,[†] Junki Kim,[†] and Dong Qin**

School of Materials Science and Engineering, Georgia Institute of Technology, Atlanta, Georgia 30332, United States

[†]These authors contributed equally to this work.

*Corresponding author: dong.qin@mse.gatech.edu

Abstract

We report the fabrication of Ag-Au cuboctahedral nanoboxes enclosed by {100} and {111} facets, respectively, through the orthogonal deposition of Au on two different facets of Ag cuboctahedra. Specifically, we titrate aqueous $HAuCl_4$ into an aqueous mixture containing Ag cuboctahedra, ascorbic acid, and NaOH (under a basic condition), in the presence of poly(vinylpyrrolidone) (PVP) and cetyltrimethylammonium chloride (CTAC), respectively. In the case of PVP, the oxidation of Ag was initiated from the {111} facets of the cuboctahedra through the galvanic replacement reaction between Au(III) and Ag, accompanied by the deposition of Au onto the {100} facets. Because the dissolved Ag(I) ions could react with NaOH to form Ag_2O on the {111} facets and thus terminate the galvanic reaction, the Au(III) ions would be further reduced by ascorbate monoanion ($HAsc^-$) to generate Au atoms for their continuing deposition on the {100} facets, converting Ag cuboctahedra to $Ag@Au_{\{100\}}$ cuboctahedra. Upon the etching of Ag from the core, we obtained Ag-Au cuboctahedral nanoboxes enclosed by {100} facets. In contrast, when CTAC was present, the oxidation of Ag through galvanic reaction could continuously proceed on {100} facets as the dissolved Ag(I) ions would react with the excessive amount of Cl^- ions derived from CTAC to produce soluble $AgCl_2^-$ ions rather than insoluable Ag_2O. As a result, the dissolved Ag(I) ions and the Au(III) would be co-reduced by $HAsc^-$ for the generation of Ag and Au atoms, followed by their co-deposition onto {111} facets for the generation of $Ag@Au_{\{111\}}$ concave cuboctahedra. After the removal of Ag from the core by etching, we obtained $Ag\text{-}Au_{\{111\}}$ cuboctahedral nanoboxes enclosed by {111} facets. Both samples of cuboctahedral nanoboxes exhibited strong optical absorption in the infrared region. Interestingly, the cuboctahedral nanoboxes enclosed by {111} facets embraced significantly enhanced catalytic activity toward the reduction of 4-nitrophenol by $NaBH_4$ relative to their counterparts encased by {100} facets.

Introduction

The shape of noble-metal nanocrystals have long been identified as a key parameter in controlling their properties toward the devlopment of applications in plasmonics and catalysis.[1-4] In particular, it is well-established that the distinctive activity and selectivity of metal nanocrystals in catalytic reactions explicitly depend on the arrangment of atoms situated on the outermost layer of different facets.[5-8] In the past, there has been a growing effort in the rational design and synthesis of metal nanocrystals with well-defined facets. Among those, seed-mediated growth of metal nanocrystals has shown remarkable success in offering a fine control over the geometry of the products by directly depositing the atoms on the facets of preformed seeds.[9-11] It is well known that the introduction of ligands into the growth solution could facilitate their selective chemisorption on different types of facets due to the differences in the binding affinity,[12] making it possible to manuever the growth rates on different facets and thus control the relative surface areas of different facets on the final products.[13, 14] For example, Xia and co-workers demonstrated the transfomration of Ag nanocubes into cuboctahedra by introducing citrate in a reaction solution to bind on the {111} facets of Ag nanocubes.[15] It was found that the Ag atoms would be preferentially deposited on the {100} facets to accelerate their growth along <100> directions, leading to the evolution of a cube into a cuboctahedron. We reported the reversible transformation between Ag nanoplates and Ag twinned cubes, elucidating the role of Cl^- ions in deterring the deposition and etching of Ag atoms along the <100> direction and allowing the deposition and etching along the <111> direction.[16, 17] Recently, Mirkin and co-workers demonstrated the generation of Au octahedra with hollow features by stabilizing the {111} facets of Au concave cubes through the underpotential deposition (UPD) of Ag^+ ions,[18] during which the growth of Au occured almost exclusively on the corners of the cubic seeds. On the other hand, many groups have demonstrated the generation of bimeallic core-frame and core-shell nanocrystals by selectively depositing the metal on the small areas of edges and the entire surfaces of preformed nanocrystal seeds with the involvement of different ligands in the reaction solutions.[19-25] Despite remarkable success, the previous studies involve the use of nanocrystal seeds, such as cubes, plates, and octahedra, with a single type of facets on their surfaces.

Herein we report the facet-selected, orthogonal deposition of Au on Ag cuboctahedra enclosed by a mix of {100} and {111} facets at a ratio of about 1:1.7 in terms of surface area. In a typical synthesis, we dispersed Ag cuboctahedra in an aqueous solution containing ascobic acid (H_2Asc),

NaOH, poly(vinylpyrrolidone) (PVP) or cetyltrimethylammonium chloride (CTAC). Our success relies on the use of PVP or CTAC to instigate the Ag oxidation on the {111} or {100} facets, respectively, making it possible to control the deposition pathways for Au atoms on the {100} or {111} facets in the orthongal manner for the generation of Ag@$Au_{\{100\}}$ cuboctahdra or Ag@Ag-$Au_{\{111\}}$ concave cuboctahedra. When the Ag in the core is subjected to removal by etching, we demonstrate the transformation of solids into Ag-$Au_{\{100\}}$ or Ag-$Au_{\{111\}}$ cuboctahedral nanoboxes with complementary surfaces.

Experimental

Chemicals and materials

Ethylene glycol (EG) was purchased from J. T. Baker. Silver trifluoroacetate (CF_3COOAg, 98%), gold(III) chloride trihydrate ($HAuCl_4 \cdot 3H_2O$, 99.9+%), sodium hydrosulfide hydrate ($NaHS \cdot xH_2O$), poly(vinylpyrrolidone) (PVP) with an average molecular weight of 29,000 (PVP–29) or 55,000 (PVP–55), aqueous hydrochloric acid (HCl, 37 wt. %), acetone (99.5+%), L-ascorbic acid (H_2Asc, 99%), sodium citrate tribasic dihydrate (citrate, 99.0+%), silver nitrate ($AgNO_3$, 99.0+%), aqueous cetyltrimethylammonium chloride solution (CTAC, 25 wt.%), and aqueous hydrogen peroxide (H_2O_2, 30wt.%), 4-nitrophenol (4-NP), and sodium borohydride ($NaBH_4$, 99.99%) were purchased from Sigma-Aldrich. Sodium hydroxide (NaOH, 98%) and acetone (HPLC grade, 99.5+%) were obtained from Alfa Aesar. All chemicals were used as received. All the aqueous solutions were prepared using DI water with a resistivity of 18.2 MΩ·cm at 25 °C.

Synthesis of Ag nanocubes

We followed the protocol reported by Xia and co-workers for the synthesis of Ag nanocubes with an average edge length of 38.1 ± 2.0 nm.[26] The as-obtained Ag nanocubes were washed with acetone and DI water twice and then dispersed in water for further use.

Synthesis of Ag cuboctahedra

We used the as-obtained Ag nanocubes as seeds to grow Ag cuboctahedra.[15] In a typical process, 34 μL of the aqueous suspension of Ag nanocubes (approximately 7.10×10^{10} particles per mL) was injected into an aqueous solution in a 23-mL glass vial containing 5 mL of PVP-55 (2 mg/mL), 100 μL of H_2Asc (0.1 M), and 50 μL of citrate (20 mM) l under magnetic stirring at room

temperature. Next, we used a syringe pump to titrate 1.5 mL of aqueous $AgNO_3$ (1 mM) into the reaction solution at a rate of 5 mL/h. Upon the completion of titration, the mixture was centrifuged at 1000 rpm for 10 min to precipitate out the larger random particles before the supernatant was centrifuged at 8000 rpm for 10 min to collect the solids. Finally, the as-prepared nanocrystals were washed with water twice before they were re-dispersed to 100 μL of water for further use. The Ag cuboctahedra had an average edge length of 47.2 ± 2.2 nm.

Synthesis of Ag@Au$_{\{100\}}$ cuboctahedra

In a typical process, 2 mL of aqueous PVP-29 (1 mM) was placed in a 23-mL glass vial, followed by the addition of 0.5 mL of aqueous H_2Asc (0.1 M), 0.5 mL of aqueous NaOH (0.2 M), and 30 μL of an aqueous suspension of the Ag cuboctahedra (approximately 4.23×10^{10} particles per mL) under magnetic stirring at room temperature. Next, we introduced 0.4 mL of aqueous $HAuCl_4$ (0.1 mM) into the reaction solution using a syringe pump at an injection rate of 1 mL/min. After the completion of titration, the reaction solution was left undisturbed for 5 min before we collected the solid products by centrifugation at 6300 rpm for 10 min and then washed with water three times prior to characterization.

Synthesis of Ag-Au$_{\{100\}}$ cuboctahedral nanoboxes

We mixed 50 μL of the as-prepared Ag@Au$_{\{100\}}$ cuboctahedra with 50 μL of aqueous NaCl (10 mM), followed by the addition of 0.7 mL of PVP-29 (1 mM) and 0.3 mL of H_2Asc (0.1 M) at room temperature. After 20 min of treatment, we collected the particles by centrifugation at 5000 rpm for 15 min, washed with water once, and then introduced the particles into 1 mL of 3% aqueous H_2O_2 at room temperature. After 3 h, the hollow particles were collected by centrifugation at 13000 rpm for 10 min, washed with water twice, and then re-dispersed in 50 μL of water for both characterization and evaluation of catalytic properties.

Synthesis of Ag@Ag-Au$_{\{111\}}$ concave cuboctahedra

In a typical process, we placed 2 mL of aqueous CTAC (0.1 M) to a 23-mL glass vial, followed by the addition of 0.5 mL of aqueous H_2Asc (0.1 M), 0.5 mL of aqueous NaOH (0.2 M), and 30 μL of an aqueous suspension of the Ag cuboctahedra (approximately 4.23×10^{10} particles per mL) under magnetic stirring at room temperature. Next, we titrated 0.8 mL of aqueous $HAuCl_4$ (0.1

mM) into the reaction solution using a syringe pump at a rate of 0.02 mL/min. Immediately after the titration, we collected the particles by centrifugation at 4800 rpm for 11 min and washed with water once for characterization and further use.

Synthesis of Ag-Au$_{\{111\}}$ cuboctahedral nanoboxes

We dispersed 50 μL of the as-prepared Ag@Au$_{\{111\}}$ cuboctahedra in 1 mL of 3% aqueous H_2O_2 for etching at room temperature. After 3 h of etching, we collected the particles by centrifugation at 13000 rpm for 10 min, washed with water twice, and then re-dispersed them in 50 μL of water for the characterization and evaluation of catalytic properties.

Catalytic characterization of Ag-Au$_{\{100\}}$ and Ag-Au$_{\{111\}}$ nanoboxes. In a typical experiment, 2 mL of aqueous 4-NP (0.2 mM), 5 mL of water, and 1 mL of aqueous $NaBH_4$ (10 mg/mL, freshly prepared, ice cold) were added into a 23-mL glass vial under magnetic stirring. After the introduction of the nanoboxes (~10^{11} particles), we monitored the reaction as a function of time by withdrawing 0.5 mL of the reaction solution to collect the UV-vis spectrum at each time point.

Instrumentation and characterization

The UV-vis spectra were collected using a Cary 50 spectrometer (Agilent Technologies, Santa Clara, CA). The UV-vis-NIR spectra were collected using a LAMDA 750 (PerkinElmer, Waltham, MA). The nanoparticles in an aqueous suspension were collected using a conventional centrifuge (Eppendorf 5430). The pH values of aqueous solutions were measured using a FE20 FiveEasy pH meter (Mettler Toledo, Columbus, OH). The quantitative measurement of Ag and Au contents in the nanocrystals was performed using an inductively-coupled plasma mass spectrometer (NexION 300Q ICP-MS, PerkinElmer, Waltham, MA). Transmission electron microscopy (TEM) images were captured using Hitachi HT7700 (Tokyo, Japan) operated at 120 kV. Scanning electron microscopy (SEM) images were captured with the Hitachi SU8230 FE-SEM (Tokyo, Japan) operated at 15-20 kV. High-angle annular dark field scanning electron microscopy and elemental mapping images were captured using the Hitachi HD2700 C_s-corrected STEM (Tokyo, Japan) operated at 200 kV.

Results and discussions

Figure 1 illustrates two proposed pathways responsible for the orthogonal deposition of Au on the {100} or {111} facets, respectively, of a Ag cuboctahedron for the generation of a Ag-$Au_{\{100\}}$ or a Ag-$Au_{\{111\}}$ cuboctahedral nanobox. In a typical synthesis, we dispersed Ag cuboctahedra in an aqueous mixture containing H_2Asc, NaOH (at an initial pH of 11.2), and either PVP or CTAC, followed by the titration of aqueous $HAuCl_4$ using a syringe pump at room temperature. Under an alkaline condition, H_2Asc would be neutralized into ascorbic monoanion ($HAsc^-$),[27] a true reducing agent. Based on our previous study,[28] we argue that the Ag atoms on the {111} facets would be initially oxidized by Au(III) to generate a small amount of Au atoms for their immediate deposition on the {100} facets (or the edges). With the involvement of NaOH in the solution, the resultant Ag(I) ions would react with OH^- for the formation of Ag_2O on the {111} facets, prohibiting the underlying Ag from further reacting with Au(III) ions. From this time point, the Au(III) ions would be reduced by HAsc- to produce more Au atoms for this subsequent deposition onto the {100} facets conformally.[29] Likely, some of the newly deposited Au atoms could migrate to the Ag_2O passivated {111} faets through surface diffusion.[30] At the end, a Ag cuboctahedron is transformed into a Ag@$Au_{\{100\}}$ cuboctahedron with the inclusion of some Au atoms on the Ag_2O regions at the {111} facets. Because Ag_2O layer can be dissolved in a weak acid,[31] we treated the as-obtained products with H_2Asc and then etched the Ag from the core with aqueous H_2O_2, leading to the conversion of the Ag@$Au_{\{100\}}$ cuboctahedron into a Ag-$Au_{\{100\}}$ cuboctahedral nanobox encased by {100} facets. It is worth noting that some NaCl was added during the weak acid treatment to increase the solubility of Ag_2O for an efficient dissolution of the Ag_2O layer.[32]

In comparison, when the PVP in the reaction solution is replaced by CTAC, the Cl^- ions derived from CTAC could strongly interact with the {100} facets, as reported by others.[33] In this case, the oxidation of Ag by Au(III) would be initiated on the {100} facets, which is orthogonal to what is involved in the PVP-based synthesis.[34] Additionally, the dissolved Ag(I) ions would form soluble $AgCl_2^-$ ions rather than react with OH^- to produce Ag_2O, due to the excessive amount of the Cl^- ions invovled in the reaction soluton.[35] As a consequence, both the $AgCl_2^-$ and Au(III) ions would be co-reduced by $HAsc^-$ into Ag and Au atoms, respectively, for their co-deposition onto the Ag cuboctahedra. Because the {100} facets are involved in the oxidation of Ag, we argue that the co-deposition of Au and Ag atoms would be mainly confined to the {111} facets. As $HAuCl_4$ is titrated into the reaction solution, more and more Ag atoms would be carved away from the {100} facets, leading to the generation of a Ag@Ag-$Au_{\{111\}}$ concave cuboctahedron. After the

etching of Ag from the core with aqueous H_2O_2, Ag-$Au_{\{111\}}$ cuboctahedral nanoboxes covered by {111} facets will be obtained.

In a typical synthesis, we first produced the Ag nanocubes with an average edge length of 38.1 ± 2.0 nm (Figure S1).[26] The as-obtained Ag nanocubes were then used as seeds to generate Ag cuboctahedra with an average edge length of 47.2 ± 2.2 nm (Figure S2).[15] In one set of study, we dispersed the Ag cuboctadedra in an aqueous solution containing H_2Asc, NaOH, and PVP, followed by the titration of aqueous $HAuCl_4$ (0.1 mM) at an initial pH of 11.2. Figure 2A shows a transmission electron microscope (TEM) image of the product prepared by adding 0.4 mL of $HAuCl_4$. Figure 2B shows an aberration-corrected high-angle annular dark-field scanning TEM (HAADF-STEM) image of a single cuboctahedron taken from the sample in Figure 2A. When aligned along the <001> zone axis, we could easily resolve the distinctive contrast between the bright region at the center and the darker regions at the four corners, which correspond to the {100} and the {111} facets of the cuboctahedron, respectively. Because the heavier Au atoms (which contribute to the mass contrast) were located on the {100} facets that are parallel with the zone axis, we observed brigher contrast at the four edges. Figure S3, A and B, shows two atomic-resolution HAADF-STEM images of the as-prepared Ag@$Au_{\{100\}}$ cuboctahedron, from which columns of atoms were visible with no significant presence of an oxide layer. We also performed energy dispersive X-ray spectroscopy (EDS) mapping on the same cuboctahedron to confirm the spatial distribution of each element. Figure 2, C and D, shows the elemental mapping of Ag and Au, respectively. We noticed that more signals from Ag were distributed at the center face than at the four corners, consistent with the thickness contrast of a cuboctahedron along the <001> zone axis. On the other hand, the signals from Au were mainly localized to the center face and the four edges but not at the four corners. The Au distribution coincides with the presence of four edges that appear brighter on the HAADF-STEM image in Figure 2B, confirming the deposition of onto the {100} and {110} surfaces. In comparison of Au signal as shown in Figure 2D, Figure S4, A and B, shows the same particle and the elemental mapping of oxygen. Because the oxygen signals were present both outside and inside the nanocrystal, we argue that it is difficult to use EDS to confirm the presence of oxide layer. Altogether, we were not able to characterize the Ag_2O layer underneath the Au by STEM and EDS. Figure 2, E and F, shows the TEM and SEM images of the final nanoboxes, from which we clearly observed the formation of {100} facets. Because all facets are well connected in a nanobox, we argue that Au deposition would also occur on the {110} facets

of the Ag cuboctahedra, serving as the vertices of cuboctahedral nanoboxes. Using inductively-coupled plasma mass spectroscopy (ICP-MS), we determined that the Ag-$Au_{\{100\}}$ nanoboxes were made of a Au-Ag alloy with a composition of $Ag_{64}Au_{36}$.

By replacing the PVP with CTAC while keeping all other parameters the same, Figure 3A shows a TEM image of the products obtained after the titration of 0.8 mL of $HAuCl_4$. Figure 3B shows a HAADF-STEM image of one nanoparticle taken from the sample in Figure 3A. The particle was oriewnted along the <001> zone axis, confirming the concave features on the {100} facets of the cuboctahedron due to the removal of Ag from these facets. As shown in Figure 3, C and D, the EDS elemental mapping of Ag and Au of the same nanoparticle indicates that the Ag signals were more intense in the center region within the concave perimeter while the Au signals were located at the edges, especially more so toward the four corners, suggesting the predomoniant deposition of Au on the {111} facets with very few on the {100} facets. Figure S5A shows a HAADF-STEM image of another nanoparticle oriented along the <111> zone axis, showing a brighter contrast at the {111} facet due to the thickness contrast. In addition, the three {100} surfaces situated at 120° angles from each other show a darker contrast, revealing their concavity. As shown by the EDS mapping in Figure S5B, the Ag signals are more intense at the center, generally following the contrast distribution in Figure S5A. Figure S5C shows that the Au signals are somewhat localized at the edges, which reflects the presence of Au atoms on the {111} facets. Away from the edges, the Au signals seem to be spread out across the particle because of the contribution of Au signals from the three {100} facets at the bottom of the cuboctahedron. After the etching of Ag from the core with aqueous H_2O_2, Figure 3, E and F, shows TEM and SEM images of the resultant nanoboxes enclosed by {111} facets, respectively, indicating that the {100} facets of concave cuboctadera would be covered by small amount of Au. The ICP-MS measurement incidates that the Ag-$Au_{\{111\}}$ nanoboxes made of of $Ag_{77}Au_{23}$. Interestingly, the composition of Au for these nanoboxes prepared with 0.8 mL of $HAuCl_4$ was lower than that in the Ag-$Au_{\{100\}}$ nanoboxes (with a composition of $Ag_{64}Au_{36}$) prepared with 0.4 mL of $HAuCl_4$ in the presence of PVP. We suspect that part of this difference arises from the co-deposition of both Ag and Au atoms on the {111} facets of the cuboctahedra during the synthesis involving CTAC.

We also used UV-vis-NIR spectroscopy to characterize the optical properties of the resultant cuboctahedral nanoboxes. When Ag@$Au_{\{100\}}$ cuboctahedra were transformed into Ag-$Au_{\{100\}}$ nanoboxes, Figure 4A shows that the localized surface-plasmon resonance (LSPR) peak was red-

shifted from from 463 nm to 1290 nm, together with the emergence of three other peaks at 845, 925, and 1140 nm. In comparison, Figure 4B shows that the major LSPR peak of Ag@Ag-Au$_{\{111\}}$ concave cuboctahedra was located at 499 nm, which is further red-shifted from that of the Ag@Au$_{\{100\}}$ cuboctahedra located at 463 nm due to the surface concavity. When they were transformed into Ag-Au$_{\{111\}}$ nanoboxes, the LSPR peak was shifted to 1305 nm with another peak appeared at 1175 nm. We could attribute the main LSPR peak of both types of nanoboxes (1295 and 1305 nm, respectively for Ag-Au$_{\{100\}}$ and Ag-Au$_{\{111\}}$) to the electric dipole mode, which has a strong correlation with the dimensions of the nanobox.[36] Unfortunately, it remains extremely challenging to measure the thickness of these nanoboxes while the composition can only be obtained by ICP-MS measurements. As such, we cannot perform the discrete dipole approximation (DDA) calculation to make assignments for specific plasmonic modes. Compared to the cubic Au nanoboxes with LSPR peak located at 1080 nm,[29] the LSPR peaks of these two types of Ag-Au cuboctahedral nanoboxes were further shifted to the infrared region.

We evaluated the catalytic activity of the cuboctahedral nanoboxes using a model reaction based on the reduction of 4-nitrophenol (4-NP) to 4-aminophenol (4-AP) by $NaBH_4$.[37] After the introduction of $NaBH_4$, we recorded the UV-vis spectra of 4-NP at different reaction time points (Figure 5, A and C). By following the intensity of the absorption peak at 400 nm, we plotted the $\ln(A_t/A_o)$ as a function of reaction time (Figure 5, B and D). In both cases, the reduction reaction exhibited first-order kinetics, from which we obtained the rate constant through curve fitting. The rate constants of Ag-Au$_{\{100\}}$ and Ag-Au$_{\{111\}}$ cuboctahedral nanoboxes were 0.005 min^{-1} and 0.213 min^{-1}, respectively, indicting distinctive catalytic activities toward this reduction reaction. We believe there are several factors that could contribute to this significant difference. Based on our ICP-MS measurements, both Ag-Au$_{\{100\}}$ and Ag-Au$_{\{111\}}$ cuboctahedral nanoboxes were made of Ag-Au alloy with a composition of $Ag_{64}Au_{36}$ and $Ag_{77}Au_{23}$, respectively. As many groups argue that Au is a more effective catalyst for the reduction of 4-NP compared to Ag,[38-43] it is possible that the difference arises from the fact that the Ag-Au$_{\{111\}}$ cuboctahedral nanoboxes may embrace Au-dominated outermost surfaces while the Ag-Au$_{\{100\}}$ cuboctahedral nanoboxes could consist of Ag-dominated surfaces. However, it is indeed extremely difficult to characterize the composition of the outermost surfaces to fully support this argument. On the other hand, we believe that the use of PVP or CTAC in the original synthesis of these nanoboxes could contribute to the different arrangement of atoms on the {100} or {111} facets of cuboctahedra, respectively, leading to their

distinct catalytic activities. Finally, it is also possible that the dissolved oxygen species in reaction solution could attribute to the different induction time of 4-NP reduction because Ag atoms could leach out into the solution as Ag ions and thus affect the catalytic performance.[44, 45]

Conclusions

We have demonstrated the transformation of Ag cuboctahedra into Ag-Au cuboctahedral nanoboxes with complementary facets by including either poly(vinylpyrrolidone) (PVP) or cetyltrimethylammonium chloride (CTAC) to a reaction solution containing Ag cuboctahedra, H_2Asc, and NaOH at the pH around 11, followed by the titration of aqueous $HAuCl_4$. When the PVP was involved, the oxidation of Ag would be initiated on the on the {111} facets for the deposition of Au on the {100} facets in the orthogonal manner, transforming Ag cuboctahedra into $Ag@Au_{\{100\}}$ cuboctahedra and then cuboctahedral nanoboxes enclosed by the {100} facets after the etching of Ag by H_2O_2. In comparison, when the CTAC was added to the reaction solution, the oxidation of Ag would continuously progress on the {100} facets for the generation of concavities. Concomitantly, the dissolved Ag(I) ions and the Au(III) would be co-reduced by chemical reduction for the generation of Ag and Au atoms, followed by their co-deposition on the {111} facets for the generation of $Ag@Au_{\{111\}}$ concave cuboctahedra and the resultant $Ag\text{-}Au_{\{111\}}$ cuboctahedral nanoboxes enclosed by {111} facets after the removal of Ag. Both types of cuboctahedral nanoboxes embrace strong LSPR properties in the infrared region. On the other hand, cuboctahedral nanoboxes enclosed by the {111} facets exhibit catalytic activities toward the reduction of 4-NP by $NaBH_4$.

Conflicts of interest

There are no conflicts to declare.

Acknowledgements

We thank the National Science Foundation (CHE-1708300) for the finacial support of this project. We also acknowledge the use of the materials characterization facility at the Institute of Electronics and Nanotechnology (IEN) at GT.

References

(1) M. Rycenga, C. M. Cobley, J. Zeng, W. Li, C. H. Moran, Q. Zhang. D. Qin, Y. Xia, Controlling the Synthesis and Assembly of Silver Nanostructures for Plasmonic Applications. *Chem. Rev.* 2011, ***111***, 3669-3712.

(2) C. J. Orendorff, T. K. Sau and C. J. Murphy, Shape-Dependent Plasmon-Resonant Gold Nanoparticles, *Small*, 2006, **2**, 636-639.

(3) N. Tian, Z.-Y. Zhou, S.-G. Sun, Y. Ding and Z. L. Wang, Synthesis of Tetrahexahedral Platinum Nanocrystals with High-Index Facets and High Electro-Oxidation Activity, *Science*, 2007, **316**, 732-735.

(4) A. R. Tao, S. Habas and P. Yang, Shape Control of Colloidal Metal Nanocrystals, *Small*, 2008, **4**, 310-325.

(5) M. H. Huang and P.-H. Lin, Shape-Controlled Synthesis of Polyhedral Nanocrystals and Their Facet-Dependent Properties, *Adv. Func. Mater.*, 2012, **22**, 14-24.

(6) C.-Y. Chiu, P.-J. Chung, K.-U. Lao, C.-W. Liao and M. H. Huang, Facet-Dependent Catalytic Activity of Gold Nanocubes, Octahedra, and Rhombic Dodecahedra toward 4-Nitroaniline Reduction, *J. Phys. Chem. C*, 2012, **116**, 23757-23763.

(7) S. Xie, S.-I. Choi, X. Xia and Y. Xia, Catalysis on faceted noble-metal nanocrystals: both shape and size matter, *Curr. Opin. Chem. Eng.*, 2013, **2**, 142-150.

(8) Q. Zhang and H. Wang, Facet-Dependent Catalytic Activities of Au Nanoparticles Enclosed by High-Index Facets, *ACS Catal.*, 2014, **4**, 4027-4033.

(9) Y. Xia, K. D. Gilroy, H.-C. Peng and X. Xia, Seed-Mediated Growth of Colloidal Metal Nanocrystals, *Angew. Chem. Int. Ed.*, 2017, **56**, 60-95.

(10) W. Niu, L. Zhang and G. Xu, Seed-mediated growth of noble metal nanocrystals: crystal growth and shape control, *Nanoscale*, 2013, **5**, 3172-3181.

(11) Y. Wu, X. Sun, Y. Yang, J. Li, Y. Zhang, D. Qin, Acc. Chem. Res., 2017, **50**, 1774-1784..

(12) A. W. Adamson and A. P. Gast, *Physical chemistry of surfaces*, Interscience New York, 1967.

(13) B. Nikoobakht and M. A. El-Sayed, Preparation and Growth Mechanism of Gold Nanorods (NRs) Using Seed-Mediated Growth Method, *Chem. Mater.*, 2003, **15**, 1957-1962.

(14) S. E. Habas, H. Lee, V. Radmilovic, G. A. Somorjai and P. Yang, Shaping binary metal nanocrystals through epitaxial seeded growth, *Nat. Mater.*, 2007, **6**, 692.

(15) Y. Wang, D. Wan, S. Xie, X. Xia, C. Z. Huang and Y. Xia, Synthesis of Silver Octahedra with Controlled Sizes and Optical Properties via Seed-Mediated Growth, *ACS Nano*, 2013, **7**, 4586-4594.

(16) J. Zhang, J. Liu, Z.-X. Xie and D. Qin, $HAuCl_4$: A Dual Agent for Studying the Chloride-Assisted Vertical Growth of Citrate-Free Ag Nanoplates with Au Serving as a Marker, *Langmuir*, 2014, **30**, 15520-15530.

(17) C.-W. Wang, X. Sun, H.-T. Chang and D. Qin, Generation of Enzymatic Hydrogen Peroxide to Accelerate the Etching of Silver Nanocrystals with Selectivity, *Chem. Mater.*, 2016, **28**, 7519-7527.

(18) M. R. Langille, M. L. Personick, J. Zhang and C. A. Mirkin, Bottom-Up Synthesis of Gold Octahedra with Tailorable Hollow Features, *J. Am. Chem. Soc.*, 2011, **133**, 10414-10417.

(19) D. Kim, Y. W. Lee, S. B. Lee and S. W. Han, Convex Polyhedral Au@Pd Core–Shell Nanocrystals with High-Index Facets, *Angew. Chem. Int. Ed.*, 2012, **51**, 159-163.

(20) S. Xie, N. Lu, Z. Xie, J. Wang, M. J. Kim and Y. Xia, Synthesis of Pd-Rh Core–Frame Concave Nanocubes and Their Conversion to Rh Cubic Nanoframes by Selective Etching of the Pd Cores, *Angew. Chem. Int. Ed.*, 2012, **51**, 10266-10270.

(21) R. G. Weiner, M. R. Kunz and S. E. Skrabalak, Seeding a New Kind of Garden: Synthesis of Architecturally Defined Multimetallic Nanostructures by Seed-Mediated Co-Reduction, *Acc. Chem. Res.*, 2015, **48**, 2688-2695.

(22) J. Li, X. Sun and D. Qin, Ag-Enriched Ag-Pd Bimetallic Nanoframes and Their Catalytic Properties, *ChemNanoMat*, 2016, **2**, 494-499.

(23) N. S. R. Satyavolu, L. H. Tan and Y. Lu, DNA-Mediated Morphological Control of Pd–Au Bimetallic Nanoparticles, *J. Am. Chem. Soc.*, 2016, **138**, 16542-16548.

(24) L. Zhang, Z. Xie, J. Gong, Shape-Controlled Synthesis of Au-Pd Bimetallic Nanocrystals for Catalytic Applications, *Chem. Soc. Rev.*, 2016, **45**, 3916-3934.

(25) X. Sun, D. Li, Y. Ding, W. Zhu, S. Guo, Z. L. Wang, S. Sun, Core/Shell Au/CuPt Nanoparticles and Their Dual Electrocatalysis for Both Reduction and Oxidation Reactions, *J. Am. Chem. Soc.*, 2014, **136**, 5745-5749.

(26) Q. Zhang, W. Li, L.-P. Wen, J. Chen and Y. Xia, Facile Synthesis of Ag Nanocubes of 30 to 70 nm in Edge Length with CF3COOAg as a Precursor, *Chem. Eur. J.*, 2010, **16**, 10234-10239.

(27) J. Du, J. J. Cullen and G. R. Buettner, Ascorbic acid: Chemistry, biology and the treatment of cancer, *Biochim. Biophys. Acta – Rev. Cancer*, 2012, **1826**, 443-457.
(28) X. Sun, J. Kim, K. D. Gilroy, J. Liu, T. A. F. König and D. Qin, Gold-Based Cubic Nanoboxes with Well-Defined Openings at the Corners and Ultrathin Walls Less Than Two Nanometers Thick, *ACS Nano*, 2016, **10**, 8019-8025.
(29) Y. Yang, J. Liu, Z.-W. Fu and D. Qin, Galvanic Replacement-Free Deposition of Au on Ag for Core–Shell Nanocubes with Enhanced Chemical Stability and SERS Activity, *J. Am. Chem. Soc.*, 2014, **136**, 8153-8156.
(30) X. Xia, S. Xie, M. Liu, H.-C. Peng, N. Lu, J. Wang, M. J. Kim and Y. Xia, On the role of surface diffusion in determining the shape or morphology of noble-metal nanocrystals, *Proc. Natl. Acad. Sci. U.S.A.*, 2013, **110**, 6669-6673.
(31) H. L. Johnston, F. Cuta and A. B. Garrett, The Solubility of Silver Oxide in Water, in Alkali and in Alkaline Salt Solutions. The Amphoteric Character of Silver Hydroxide, *J. Am. Chem. Soc.*, 1933, **55**, 2311-2325.
(32) X. Li, J. J. Lenhart, H. W. Walker, Aggregation Kinetics and Dissolution of Coated Silver Nanoparticles.
(33) S. Zhou, J. Li, K. D. Gilroy, J. Tao, C. Zhu, X. Yang, X. Sun and Y. Xia, Facile Synthesis of Silver Nanocubes with Sharp Corners and Edges in an Aqueous Solution, *ACS Nano*, 2016, **10**, 9861-9870.
(34) J. Ahn, D. Wang, Y. Ding, J. Zhang, D. Qin, Site-Selective Carvings and Co-Deposition: Transformation of Ag Nanocubes into Concave Nanocrystals Encased by Au-Ag Alloy Frames, *ACS Nano*, 2018, **12**, 298-307.
(35) J. Du, Z. Chen, C. Chen, T. J. Meyer, A Half-Reaction Alternative to Water Oxidation: Chloride Oxidation to Chlorine Catalyzed by Silver Ion, *J. Am. Chem. Soc.*, 2015, **137**, 3193-3196.
(36) A. M. Schwartzberg, T. Y. Olson, C. E. Talley, J. Z. Zhang, Synthesis, Characterization, and Tunable Optical Properties of Hollow Gold Nanospheres, *J. Phys. Chem. B*, 2006, **110**, 19935-19944.
(37) N. Pradhan, A. Pal and T. Pal, Catalytic Reduction of Aromatic Nitro Compounds by Coinage Metal Nanoparticles, *Langmuir*, 2001, **17**, 1800-1802.

(38) P. Xu, L. Kang, N. H. Mack, K. S. Schanze, X. Han and H.-L. Wang, Mechanistic understanding of surface plasmon assisted catalysis on a single particle: cyclic redox of 4-aminothiophenol, *Sci. Rep.*, 2013, **3**, 2997.

(39) J. Li, J. Liu, Y. Yang and D. Qin, Bifunctional Ag@Pd-Ag Nanocubes for Highly Sensitive Monitoring of Catalytic Reactions by Surface-Enhanced Raman Spectroscopy, *J. Am. Chem. Soc.*, 2015, **137**, 7039-7042.

(40) P. Zhao, X. Feng, D. Huang, G. Yang, D. Astruc, Basic Concepts and Recent Advances in Nitrophenol Reduction by Gold- and Other Transition Metal Nanoparticles, *Coord. Chem. Rev.*, 2015, **287**, 114-136.

(41) Y. Shin, A. Dohnalkova, Y. Lin, Preparation of Homogeneous Gold-Silver Alloy Nanoparticles Using the Apoferritin Cavity as a Nanoreactor, *J. Phys. Chem. C*, 2010, **114**, 5985-5989.

(42) L. Sun, P. Lv, H. Li, F. Wang, W. Su, L. Zhang, One-Step Synthesis of Au-Ag Alloy Nanoparticles Using Soluble Starch and Their Photocatalytic Performance for 4-Nitrophenol Degradation, *J. Mater. Sci.*, 2018, **53**, 15895-15906.

(43) L. Sun, Y. Yin, F. Wang, W. Su, L. Zhang, Facile One-Pot Green Synthesis of Au-Ag Alloy Nanoparticles Using Sucrose and Their Composition-Dependent Photocatalytic Activity for The Reduction of 4-Nitrophenol, *Dalton Trans.*, 2018, **47**, 4315-4324.

(44) E. Menumerov, R. A. Hughes, S. Neretina, One-Step Catalytic Reduction of 4-Nitrophenol through the Direct Injection of Metal Salts into Oxygen-Depleted Reactants, *Catal. Sci. Technol.,* 2017, **7**, 1460-1464.

(45) E. Menumerov, R. A. Hughes, S. D. Golze, R. D. Neal, T. B. Demille, J. C. Campanaro, K. C. Kotesky, S. Rouvimov, S. Neretina, Identifying the True Catalyst in the Reduction of 4-Nitrophenol: A Case Study Showing the Effect of Leaching and Oxidative Etching Using Ag Catalysts, *ACS Catal.*, 2018, **8**, 8879-8888.

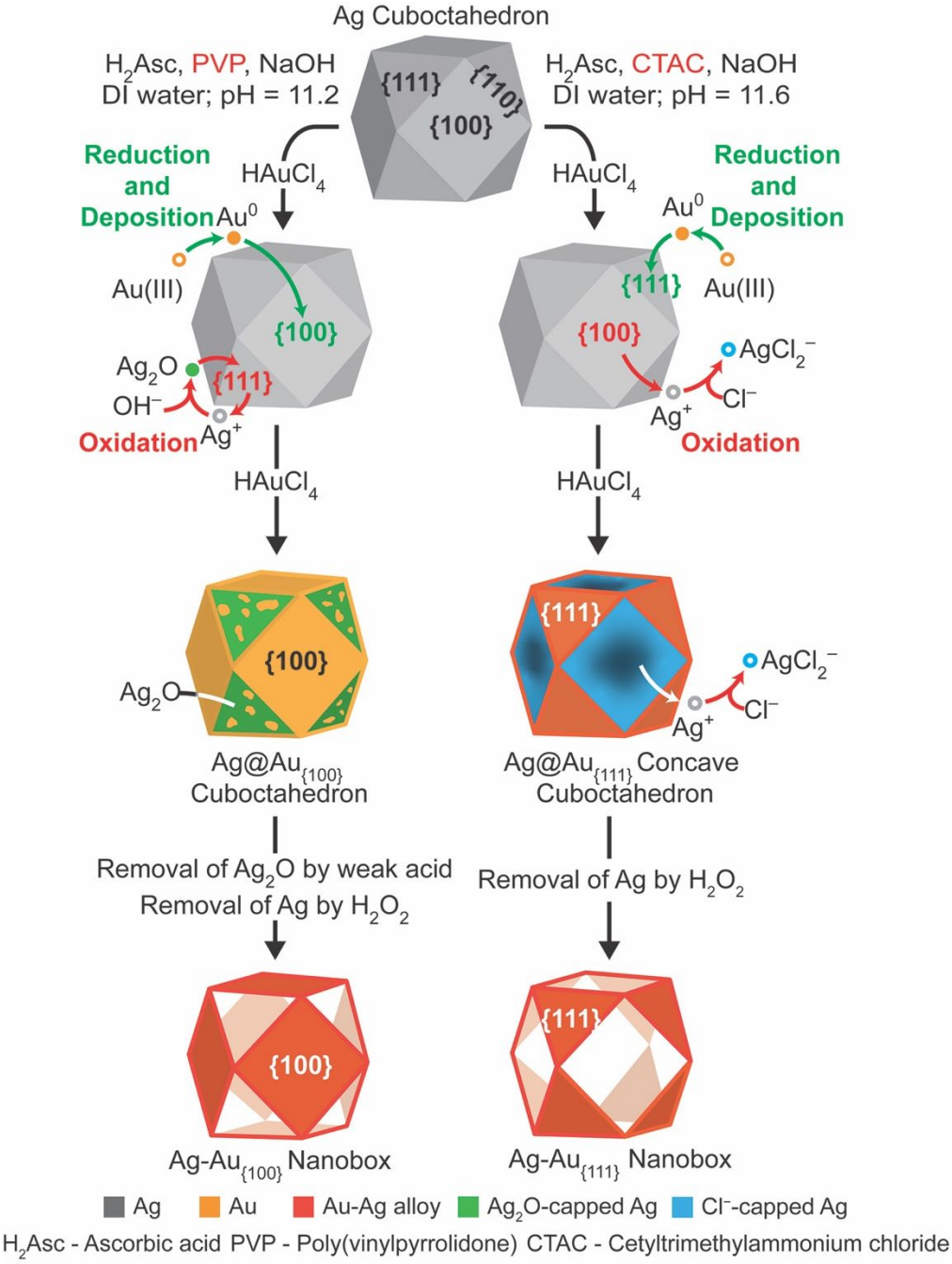

Figure 1. Schematic diagram that illustrates the two orthogonal pathways for the deposition of Au on Ag cuboctahedra in the presence of PVP and CTAC, respectively, followed by the removal of Ag for the production of cuboctahedral nanoboxes with complementary facets.

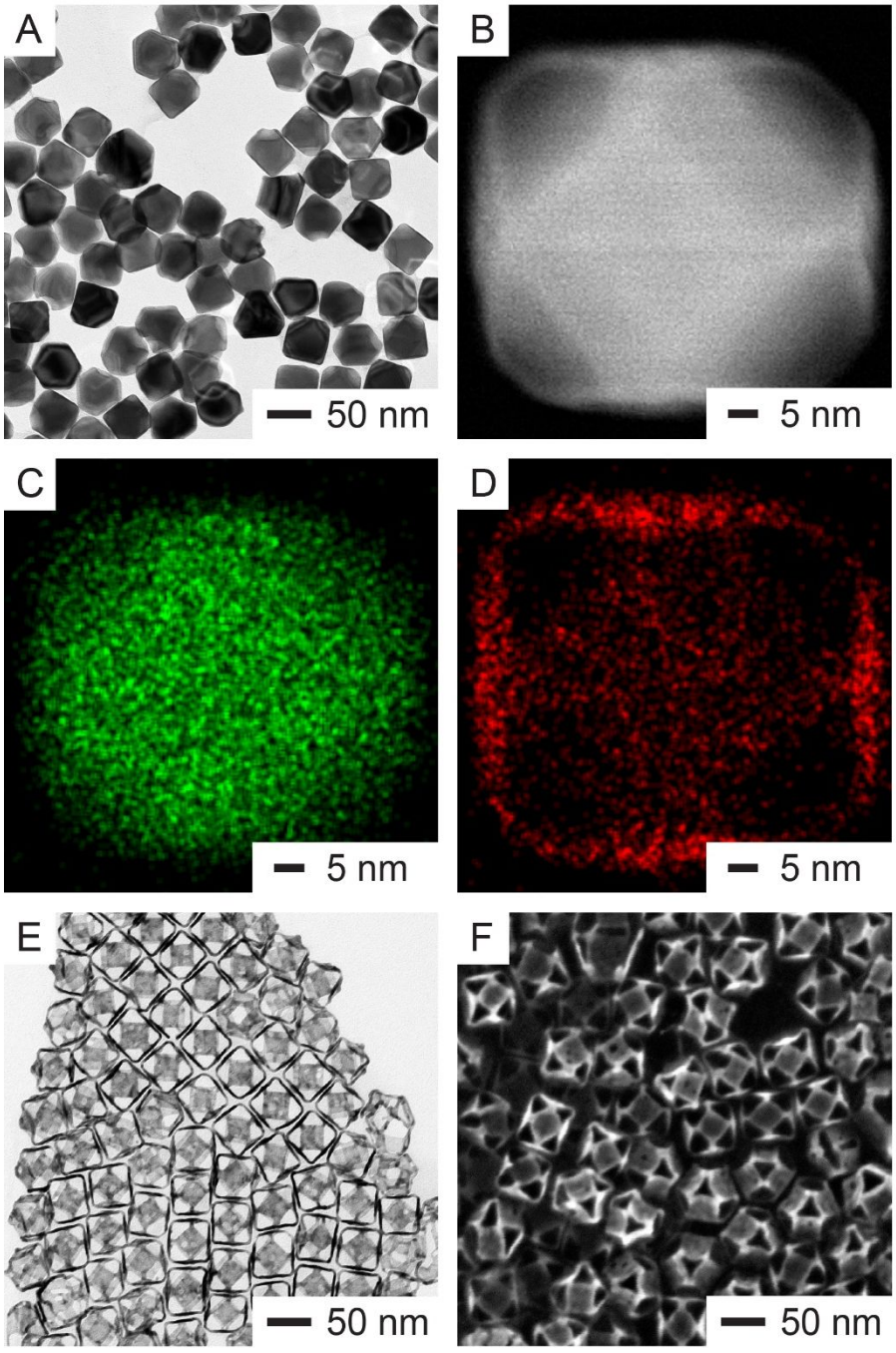

Figure 2. (A) TEM image of the as-prepared Ag@$Au_{\{100\}}$ cuboctahedra. (B) HAADF-STEM image of one nanocrystal that was orientated along the <001> zone axis. (C, D) EDS mapping of the same nanocrystal (green: Ag; red: Au). (E) TEM and (F) SEM images of the resultant Ag-$Au_{\{100\}}$ cuboctahedral nanoboxes after the removal of Ag.

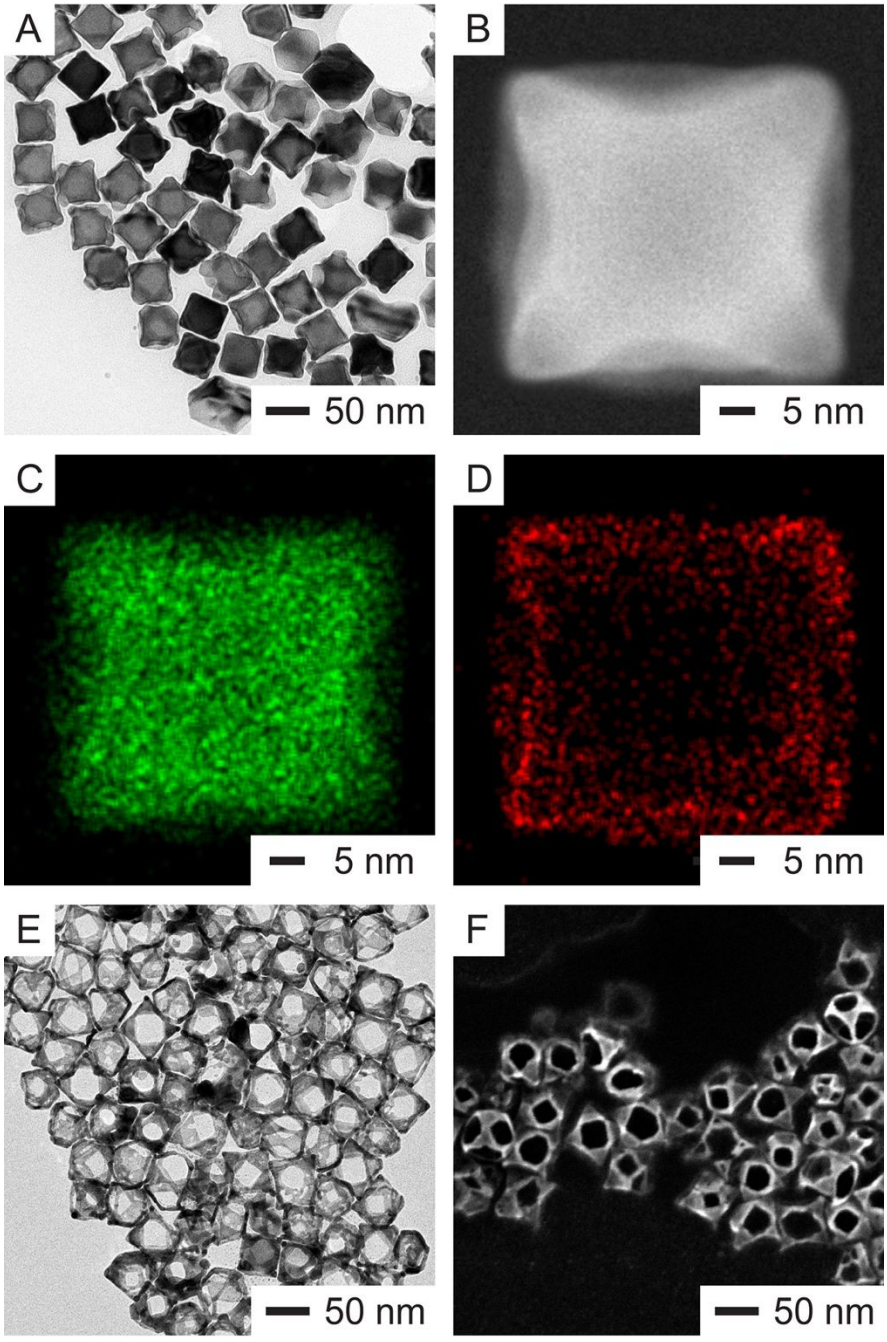

Figure 3. (A) TEM image of the as-prepared Ag@Ag-$Au_{\{111\}}$ concave cuboctahedra. (B) HAADF-STEM image of one nanocrystal that was orientated along the <001> zone axis. (C, D) EDS mapping of the same nanocrystal (green: Ag; red: Au). (E) TEM and (F) SEM images of the resultant Ag-$Au_{\{111\}}$ cuboctahedral nanoboxes after the etching of Ag.

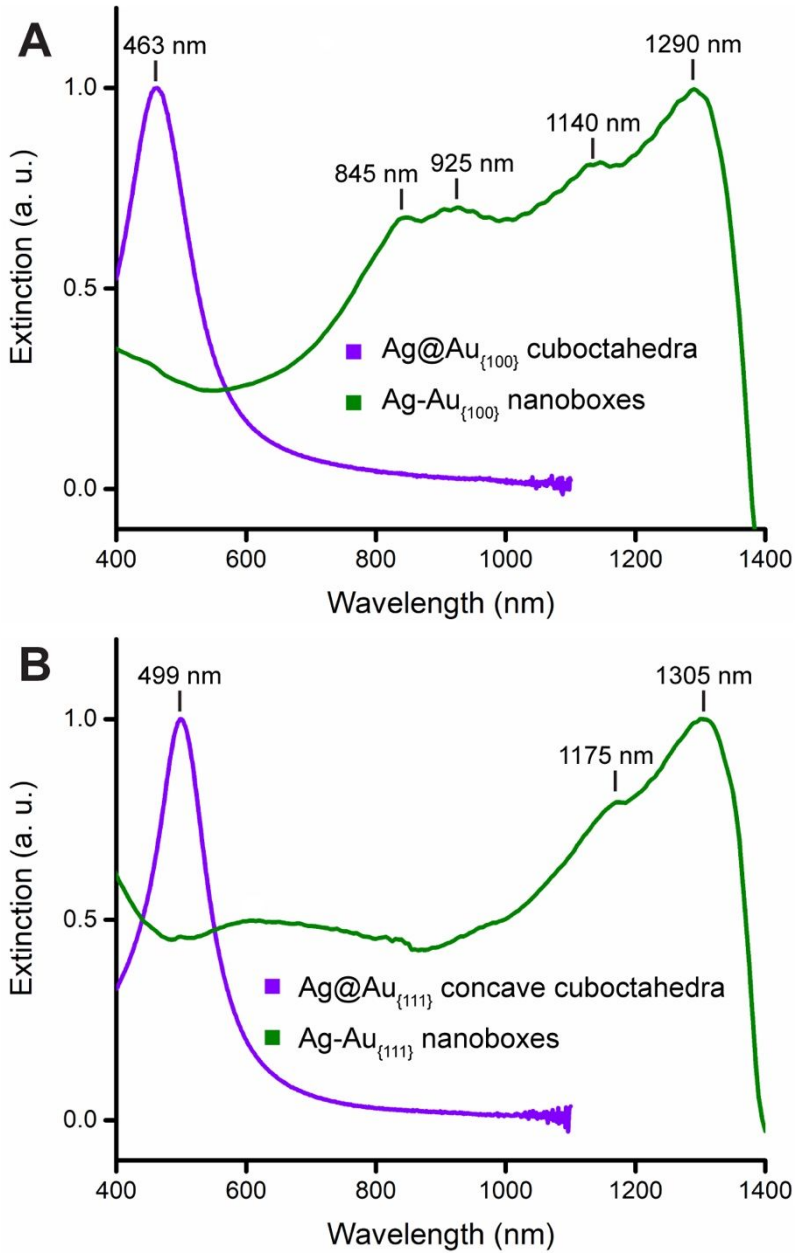

Figure 4. (A) UV-vis spectra of the Ag@Au$_{\{100\}}$ cuboctahedra and corresponding Ag-Au$_{\{100\}}$ nanoboxes. (B) UV-vis spectra of the Ag@Ag-Au$_{\{111\}}$ concave cuboctahedra and corresponding Ag-Au$_{\{111\}}$ nanoboxes. Each spectrum was normalized to its maximum intensity.

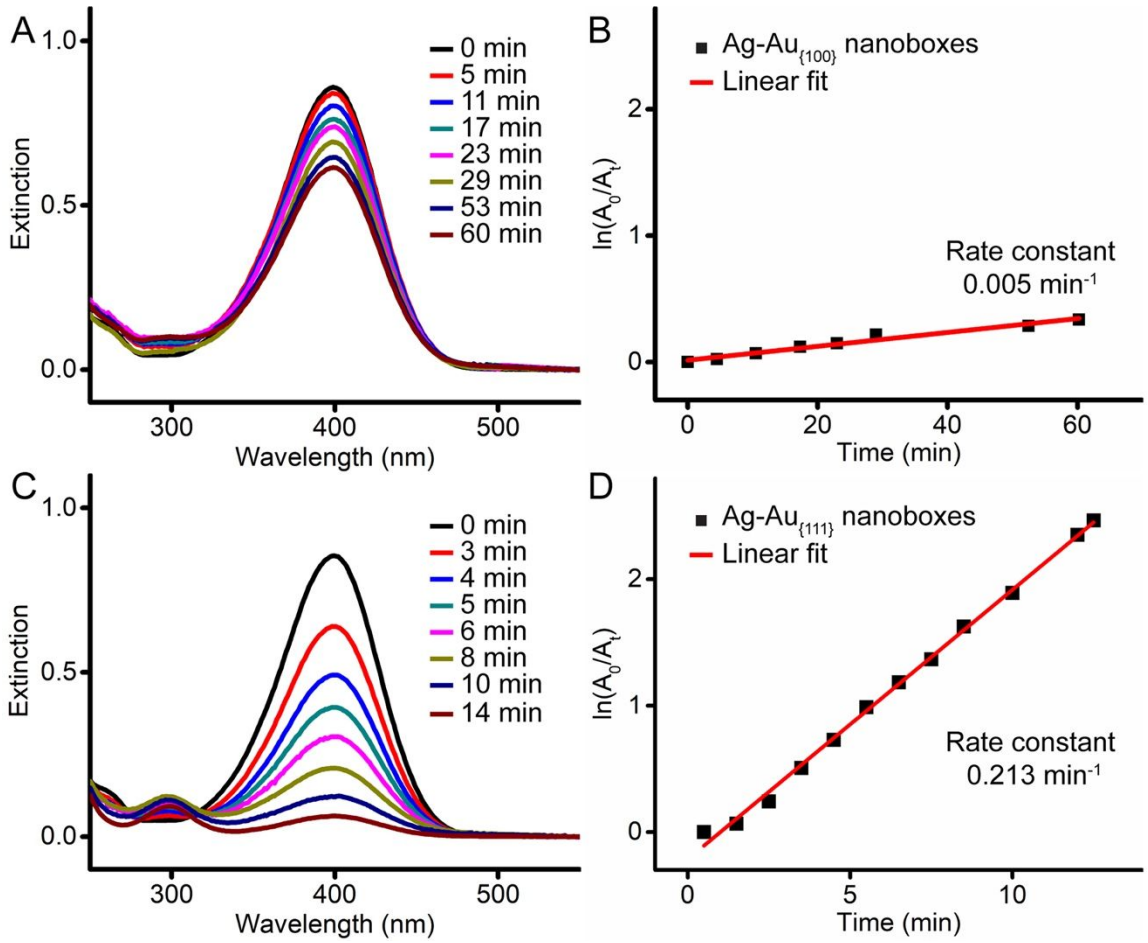

Figure 5. (A, C) UV-vis spectra recorded at different time points for the reduction of 4-NP by $NaBH_4$ at room temperature, when the Ag-$Au_{\{100\}}$ and Ag-$Au_{\{111\}}$ nanoboxes were used as the catalysts, respectively. (B, D) Plots of $\ln(A_0/A_t)$ as a function of time for the peaks located at 400 nm in (A) and (C), respectively.

TOC

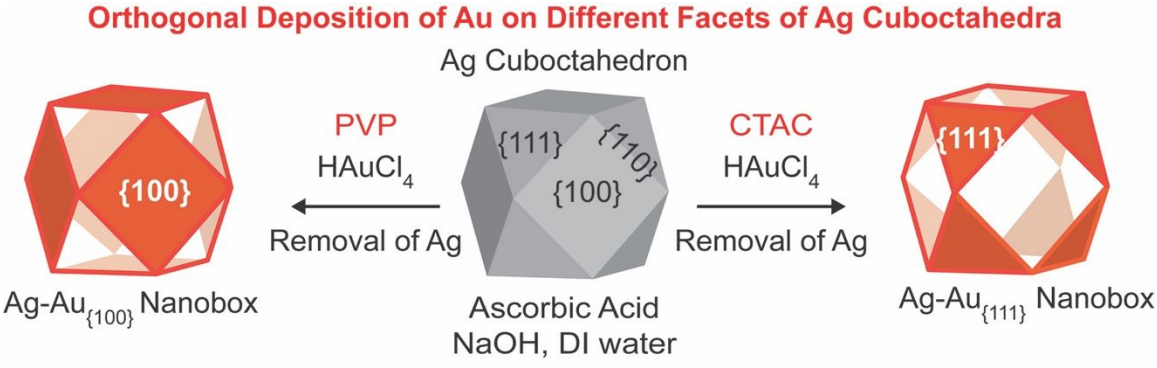
Orthogonal Deposition of Au on Different Facets of Ag Cuboctahedra
Ag Cuboctahedron
{100}
PVP
HAuCl4
Removal of Ag
{111}
{110}
{100}
CTAC
HAuCl4
Removal of Ag
{111}
Ag-Au{100} Nanobox
Ascorbic Acid
NaOH, DI water
Ag-Au{111} Nanobox